JOURNAL OF COMPUTATIONAL PHYSICS 57, 210–228 (1985)

Computation of Natural Convection in Two-Dimensional Cavities with Chebyshev Polynomials

P. LE QUERE* AND T. ALZIARY DE ROQUEFORT†

*Laboratoire d'Energetique Solaire du CNRS, and †Laboratoire d'Etudes Aerodynamiques LA 191, 40 Av. du Recteur Pineau, 86022 Poitiers Cedex, France

Received April 13, 1983; revised February 1, 1984

A semi-implicit spectral method for the computation of buoyancy induced two-dimensional flow of a viscous incompressible fluid is presented. The incompressible Navier–Stokes equations expressed in terms of the primitive variables velocity and pressure, and an additional equation for the temperature, are considered. All the variables are expanded in double truncated series of Chebyshev polynomials. The pressure distribution at the boundary of the computational domain is determined by means of an influence matrix technique in order to satisfy the incompressibility condition everywhere in the field. The algorithm is applied to the classical problem of natural convection of a Boussinesq fluid within a differentially heated vertical square cavity. Results show that, for a Prandtl number of 0.71 corresponding to air and up to Rayleigh numbers of 10^6, very accurate solutions are obtained with a spatial resolution of 33 polynomials in each direction. New interesting phenomena are shown for higher values of the Rayleigh number. © 1985 Academic Press, Inc.

1. INTRODUCTION

Spectral methods in computational fluid mechanics seem a promising alternative to more classical finite difference or finite element techniques. Most of the early work was done with Fourier series as basis functions which, unfortunately, are restricted to simple geometries and periodic boundary conditions. It was first shown by Orszag [1, 2] that, for viscous flows, the no-slip wall condition can be handled by using Chebyshev polynomials as basis expansion functions. These polynomials yield expansions the rate of convergence of which depends only on the regularity of the solution within the domain, while keeping the efficiency of the fast Fourier transforms to travel back and forth between physical and spectral space. Owing to their high accuracy, Chebyshev spectral methods seem therefore particularly suited to the study of transition to turbulence in near-to-wall flows, and among these, the problem of natural convection within differentially heated cavities is certainly one of the most challenging.

The problem of natural convection of a Boussinesq fluid in an upright two-dimensional cavity of width L and height H is entirely prescribed with three dimensionless parameters, the Rayleigh number Ra, the Prandtl number of the fluid Pr and the aspect ratio $A = H/L$ of the cavity. In the case of air ($\mathrm{Pr} = 0.71$) contained

0021-9991/85 $3.00
Copyright © 1985 by Academic Press, Inc.
All rights of reproduction in any form reserved.

within a square cavity ($A = 1$), the Rayleigh number that corresponds to the end of the steady laminar regime is not known with certainty. On the basis of a linear stability analysis of the buoyancy layer, Gill and Davey [3] place this critical Rayleigh number in the vicinity of 2×10^7, and consequently there have been very few attempts to obtain numerical solutions with $A = 1$ and $\mathrm{Pr} = 0.71$ when the Rayleigh number exceeds 10^7. Therefore, since our long-term objective is to simulate transition to turbulence of natural convection flows within cavities, we propose to integrate the time-dependent Navier–Stokes equations of a Boussinesq fluid. This paper is essentially devoted to the presentation of the numerical algorithm, and the purpose of the results given in Section 4 is, first, to validate the code by comparison with the benchmark solution of De Vahl Davis [4] and second, to indicate some new interesting features of the flow field for values of the Rayleigh number larger than 10^7.

For the computation of incompressible two-dimensional flows, it is well known that, considering the storage and also the computational requirements, the stream function and vorticity formulation seems the best choice. However, keeping in mind our interest in time-dependent flows and transition towards turbulence, we prefer to use the primitive variables velocity and pressure because they allow a more straightforward extension to three-dimensional configurations. One may also notice that if the vorticity-stream function approach was retained, the analysis and understanding of a turbulent solution would presumably need the computation of the velocity and pressure fields.

When using expansions in Chebyshev polynomials for the computation of time-dependent problems, one may encounter a first difficulty, namely, the fact that, for usual explicit time-stepping schemes, stability criteria impose a very severe limitation on the time step. The most drastic limitation comes from the diffusive stability limit, and one can show [5] that for a one-dimensional diffusion problem the critical time step is of the order of $1/\nu N^4$, where ν is the coefficient of the diffusion terms and N is the number of Chebyshev polynomials in the expansion. This limitation is quite prohibitive for long-term integration, and it is therefore necessary to resort to an implicit or semi-implicit treatment of the diffusive terms that appear in the Navier–Stokes equations.

A second difficulty comes from the lack of natural boundary conditions for the pressure. Usually one applies the divergence operator to the momentum equations in order to obtain a Poisson equation for the pressure taking into account the continuity equation. Using the no-slip condition, a direct evaluation of the normal momentum equation at a solid wall gives Neumann boundary conditions for the pressure. This procedure has been successfully applied in many finite-difference schemes. However Moin and Kim [6] showed that this procedure gives serious numerical difficulties for Chebyshev spectral methods with an explicit time integration. The problem comes from the fact that a simultaneous enforcement of the velocity boundary conditions as well as the continuity equation at the wall may lead to non-convergent series expansions for the time derivatives of the velocity components. The remedy they adopted was to consider an implicit coupled dis-

cretisation in which the pressure appears also as an unknown at the new time level. They have then to solve block systems of linear equations for the coupled velocity and pressure fields. This method was applied in the particular context of 3-D simulations of transition to turbulence between parallel planes with a 1-D Chebyshev expansion in the direction normal to the planes. A direct extension of this technique to 2-D Chebyshev expansions looks cumbersome and would result in very large systems of linear equations. For the same basic geometrical configuration Orszag and Kells [7] resorted to time-splitting techniques, which however result in a low order (typically $O(\Delta t)$) time-stepping scheme. In particular McLaughlin and Orszag [8], using the same algorithm for the study of time-dependent flow in a Rayleigh–Benard problem, found that it was necessary to use a Richardson extrapolation to recover sufficient accuracy in time. Kleiser and Schumann [9] have solved the difficulty by an influence matrix technique, and the method we have used is an extension of their algorithm to a 2-D geometrical configuration.

Throughout this paper we will use the standard terminology of spectral methods as defined, for instance, in Ref. [5].

2. Physical Problem and Equations

Let us consider the motion of a buoyant Boussinesq fluid within a two-dimensional square cavity of width L shown on Fig. 1. The direction of gravity is along the z-axis and the physical boundary conditions are:

— no-slip condition for the velocity on the four walls $EFGH$.

— constant and uniform temperatures T_1 and T_0 ($T_1 > T_0$) on the side walls FG and EH, respectively.

— perfectly insulating upper and lower walls EF and GH.

Let u and w be respectively the velocity components along the x and z axis and T the temperature. Distances and velocity components are made dimensionless using L as a reference length and a/L as a reference velocity, where a is the thermal diffusivity of the fluid. The scaled temperature θ is defined as $(T-T_0)/(T_1-T_0)$. After

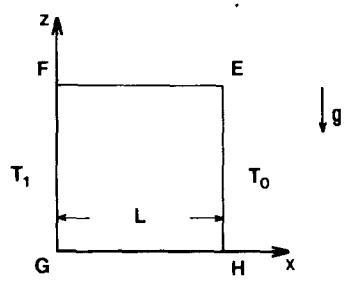

Fig. 1. Geometrical configuration

introduction of the dimensionless variables, the governing equations take the form

$$\frac{\partial\theta}{\partial t}+\frac{\partial u\theta}{\partial x}+\frac{\partial w\theta}{\partial z}=\Delta\theta \tag{1-1}$$

$$\frac{\partial u}{\partial t}+\frac{\partial u^2}{\partial x}+\frac{\partial uw}{\partial z}=-\frac{\partial P}{\partial x}+\mathrm{Pr}\,\Delta u \tag{1-2}$$

$$\frac{\partial w}{\partial t}+\frac{\partial uw}{\partial x}+\frac{\partial w^2}{\partial z}=-\frac{\partial P}{\partial z}+\mathrm{Pr}\,\Delta w+\mathrm{Ra}\cdot\mathrm{Pr}\cdot(\theta-0.5) \tag{1-3}$$

$$\frac{\partial u}{\partial x}+\frac{\partial w}{\partial z}=0 \tag{1-4}$$

where P is the non-dimensional deviation from the hydrostatic pressure. In the above equations Pr is the Prandtl number of the fluid and Ra the Rayleigh number defined as

$$\mathrm{Ra}=\frac{g\beta L^3(T_1-T_0)}{va}$$

where g is the acceleration due to gravity, β is the coefficient of thermal expansion and v is the kinematic viscosity. In the dimensionless coordinates the computational domain is the square $[0,1]\times[0,1]$ and the boundary conditions we consider read then

$$\begin{aligned}
&u, w=0 \quad \text{on} \quad x=0,1;\ 0\leqslant z\leqslant 1 \text{ and on } z=0,1;\ 0\leqslant x\leqslant 1\\
&\theta=1 \quad \text{on} \quad x=0;\quad 0\leqslant z\leqslant 1\\
&\theta=0 \quad \text{on} \quad x=1;\quad 0\leqslant z\leqslant 1\\
&\frac{\partial\theta}{\partial z}=0 \quad \text{on} \quad z=0,1;\ 0\leqslant x\leqslant 1.
\end{aligned} \tag{1-5}$$

We assume that initial conditions for $t=0$ are given.

3. Numerical Scheme

3.1. *General Formulation*

Owing to the geometry of the computational domain and to the nature of the boundary conditions imposed on the four limiting walls, all the variables are expanded in double truncated series of Chebyshev polynomials. Let $f(x, z, t)$, where f is any of the four variables u, w, P or θ, be approximated as

$$f(x,z,t)\approx f_{LM}(x,z,t)=\sum_{l=0}^{L}\sum_{m=0}^{M} f_{lm}(t)\,T_l(2x-1)\,T_m(2z-1). \tag{2}$$

Marching in time is done by a finite-difference technique, and, as already stated, the very high resolution of Chebyshev polynomials near the solid boundaries makes it necessary to resort to implicit or semi-implicit treatment of the diffusive terms in the momentum and energy equations. A very popular time-stepping scheme that achieves formally a second-order accuracy in time for the integration of an advection-diffusion equation of a scalar passive field such as Eq. (1-1) is obtained by combining an Adams–Bashforth time stepping for the convective part with a Crank–Nicolson procedure for the diffusive part. This time-stepping procedure, hereafter referred to as *ABCN*, when applied to a transport-diffusion equation of a two-dimensional scalar field $f(x, z, t)$ results in (L stands for the transport operator in divergence form)

$$\frac{f^{n+1}-f^n}{\Delta t}+\frac{3}{2}L(f)^n-\frac{1}{2}L(f)^{n-1}=\frac{1}{2}(\Delta f^{n+1}+\Delta f^n) \tag{3}$$

which can be cast into the form

$$(\Delta f-\lambda f)^{n+1}=2S_f^{n,n-1} \tag{4}$$

where $\lambda=2/\Delta t$ and $S_f^{n,n-1}$ stands for all the known quantities that depend on time levels $n\,\Delta t$ and $(n-1)\,\Delta t$.

This 2-D Helmholtz equation can be solved very efficiently with a computational algorithm proposed by Gottlieb and Orszag [5] and Haidvogel and Zang [10]. Equation (4) is solved in the transformed space of spectral coefficients and the boundary conditions are imposed with the tau method. The algorithm consists of a diagonalization of one of the two partial second derivatives operators, which is done by expressing the solution on the basis of the eigenfunctions of the corresponding operator with specified boundary conditions. The resulting linear system of equations can be cast in a quasi-tridiagonal form and solved with a specially tailored elimination procedure. Given the temperature and velocity fields at time levels $n\,\Delta t$ and $(n-1)\,\Delta t$, this computational procedure can readily be applied to determine the new temperature field governed by Eq. (1-1) at time level $(n+1)\,\Delta t$. For the computation of the source term $S_\theta^{n,n-1}$, the non-linear terms coming from the transport operator are evaluated with the classical pseudo-spectral transform method as described, for instance, in [16].

3.2. *Boundary Conditions for the Pressure*

When one wants to apply this *ABCN* scheme to the momentum equations, which have to be solved subjected to the incompressibility constraint that the divergence of the new velocity field at time level $(n+1)\,\Delta t$ should be zero, one is confronted with the difficult problem of the pressure determination. The difficulty in this case stems primarily from the implicit treatment of the viscous terms in the momentum equations. When we apply the *ABCN* scheme to the momentum equations (1–2),

(1–3), considering the pressure as an intermediate field evaluated at $(n+1/2)\,\Delta t$, we have to solve

$$\frac{\mathbf{V}^{n+1}-\mathbf{V}^{n}}{\Delta t}+\frac{3}{2}\,L(\mathbf{V})^{n}-\frac{1}{2}\,L(\mathbf{V})^{n-1}=-\nabla P^{n+1/2}+\frac{1}{2}\,(\Delta\mathbf{V}^{n+1}+\Delta\mathbf{V}^{n}) \tag{5}$$

together with the incompressibility constraint $\operatorname{div}\mathbf{V}^{n+1}=0$. For the sake of clarity, we have set the Prandtl number Pr to 1 and omitted the body force term in (1-3). Applying the divergence operator to Eq. (5) gives a Poisson's equation for the pressure which reads

$$\frac{1}{2}\,\Delta\omega^{n+1}-\frac{1}{\Delta t}\,\omega^{n+1}=\Delta P^{n+1/2}+\operatorname{div}\mathbf{S}^{n,n-1} \tag{6}$$

where ω stands for div $\mathbf{V}$, and $\mathbf{S}$ represents the vector (S_u, S_w). The only possible treatment that avoids iterating is to set the left hand side of Eq. (6) to zero. Once the pressure field is obtained and plugged back into (5), one can then advance the velocity field from time level $n\,\Delta t$ to time level $(n+1)\,\Delta t$, but it is clear that, due to the implicit treatment of the viscous terms, the divergence of the new velocity field is not zero, but satisfies the homogeneous Helmholtz equation

$$(\Delta\omega-\lambda\omega)^{n+1}=0 \qquad \text{where} \quad \lambda=2/\Delta t. \tag{7}$$

If one remarks that (7) has the unique trivial solution $\omega=0$ everywhere within the computational domain D, if and only if ω is zero on the boundary ∂D of the computational domain, the set A of equations we have to solve is

$$\Delta P+\operatorname{div}\mathbf{S}=0 \qquad \text{in } D \tag{A-1}$$

$$\Delta\mathbf{V}-\lambda\mathbf{V}=2\cdot(\nabla P+\mathbf{S}) \qquad \text{in } D \tag{A-2}$$

$$\mathbf{V}=0 \qquad \text{on } \partial D \tag{A-3}$$

$$\operatorname{div}\mathbf{V}=0 \qquad \text{on } \partial D. \tag{A-4}$$

This set of equations clearly shows that we have too many boundary conditions for the velocity and none natural for the pressure. The algorithm presented in [9] consists of considering a set B of equations, formed with (A-1), (A-2), (A-3), and (A-4) replaced by (B-4), $P=\bar{p}$ on ∂D. Throughout the rest of the paper, overbarred variables will refer to distributions on the boundary ∂D of the computational domain D.

$$\Delta P+\operatorname{div}\mathbf{S}=0 \qquad \text{in } D \tag{B-1}$$

$$\Delta\mathbf{V}-\lambda\mathbf{V}=2\cdot(\nabla P+\mathbf{S}) \qquad \text{in } D \tag{B-2}$$

$$\mathbf{V} = 0 \qquad \text{on } \partial D \tag{B-3}$$

$$P = \bar{p} \qquad \text{on } \partial D. \tag{B-4}$$

The two problems described by sets A and B will be equivalent and their solutions identical, if we can find a pressure distribution $\bar{p}$ on the boundary that produces a velocity field whose divergence is zero at the boundary and consequently everywhere within the computational domain. Having dropped (A-4) in favor of (B-4) results in that (B-1), (B-4) and (B-2), (B-3) form two Helmholtz equations with appropriate boundary conditions that can be solved independently and consecutively once S is known. Note also that in problem B, we deal with a Poisson's equation for pressure with Dirichlet type boundary conditions and escape the well-known compatibility condition when dealing with Neumann type boundary conditions.

It is possible to find this correct pressure distribution at the boundary through the use of a superposition algorithm that consists of solving first set B with a trial pressure distribution at the boundary $\bar{p}_t$, deducing the divergence of the velocity field at the boundary $\bar{\omega}_t$, and implementing a correction technique to get the correcting pressure distribution $\bar{p}_c$ at the boundary that, added to $\bar{p}_t$, gives the exact pressure distribution at the boundary. Starting from the pressure distribution at the boundary, we first solve a Poisson's equation to get the pressure field and then a Stokes problem to get the velocity field. Since these two operators are linear for a given source term S, the correspondance between the pressure distribution at the boundary and the divergence of the velocity field at the boundary is linear. Given the divergence of the velocity field at the boundary that corresponds to the trial pressure distribution, it is then possible to obtain the correcting pressure distribution at the boundary $\bar{p}_c$ through the solution of a linear system of equations. The matrix of this linear system of equations will hereafter be called the influence matrix.

It is clear that this matrix can be generated by solving homogeneous B problems ($\mathbf{S} = 0$) with $P = \bar{p}_k$ on ∂D, when $\bar{p}_k$ spans the basis of an appropriate vector space. Such an homogeneous B problem with $P = \bar{p}_k$ on ∂D will hereafter be referred to as B_k. We have to first determine the order of this matrix, and since it depends on the particular domain under consideration, we will assume that we are working in the "unit" square $[-1, 1] \times [-1, 1]$ and for the sake of simplicity we will assume $L = M$ in (2). A continuous function on the boundary of D can thus be characterized by $4L$ coefficients whether it is considered in the space of Chebyshev coefficients or through its values at the collocation points that belong to the boundary. It is natural to consider the canonical basis associated to the Chebyshev collocation points, since these points have already been introduced in the pseudo-spectral procedure of evaluation of the non-linear terms. Since the velocity is zero on ∂D, its divergence is identically zero at the four corners of the square, and this reduces the dimension of the space to which belongs the divergence on ∂D to $4(L-1) = K$. This, in turn, implies that the trial pressure distribution $\bar{p}_t$ and the correction

pressure distribution $\bar{p}_c$ are not fully arbitrary, but must obey the following relationships, which are obtained from a direct evaluation of Eq. (B-1) at each of the four corners, and account for the fact that the Laplacian of a function at the corners depends only on its boundary values

$$\left.\begin{aligned} \Delta\bar{p}_t + \operatorname{div} \mathbf{S} = 0 \\ \Delta\bar{p}_c = 0 \end{aligned}\right\} \text{ at the four corners of } D. \qquad \begin{matrix} (8\text{-}1) \\ (8\text{-}2) \end{matrix}$$

Thus, since $\bar{p}_c$ is a linear combination of the $\bar{p}_k$'s, each $\bar{p}_k$ must satisfy individually (8-2) at the 4 corners. Since all the B_k problems differ only in $\bar{p}_k$, we have to determine K distributions that are linearly independent and satisfy (8-2). We can determine them directly through their coefficients in the spectral space or through their values at the collocation points that belong to the boundary. We have chosen the second alternative for reasons that will be explained below. If we introduce the set $\{C_i\}$ of collocation points that belong to the boundary minus the four corners (there are K such points), then we can set $\bar{p}_k(C_i) = \delta_{ki}$. The values of $\bar{p}_k$ at the corners are then determined so that (8-2) is satisfied (see Appendix).

The influence matrix is then built after having solved each of the K B_k problems by juxtaposing columnwise the values of the divergence of the velocity field at the points C_i. In fact this matrix is singular; the sum of all the $\bar{p}_k$'s is obviously the unit pressure distribution on ∂D, and hence everywhere in D, and results in a zero velocity field. One has then to introduce a linearly independent equation, which is equivalent to fixing a prescribed value to the pressure field at some particular point of the computational domain. This influence matrix Q can be built and inverted once and for all in a preprocessing stage. The amount of overhead work, which is roughly equivalent to K time steps plus the matrix inversion, is always negligible in view of the total number of time steps involved in practical computations. One last important point to mention in relation to the building of this influence matrix is that, since its order can be quite large (124 if $L = M = 32$, 252 if $L = M = 64$ and the matrix is full), it has to be well conditioned to be easily invertible. This is so because of the way we picked the $\bar{p}_k$'s: a pointwise excitation in pressure results in a velocity field whose divergence is large in magnitude in the neighbourhood of this point, thus leading to a matrix than can easily be inverted with a simple Gaussian elimination.

3.3. *Computational Cycle*

We can now give a description of the computational cycle that is used to advance in time Eqs. (1-1) to (1-4).

1. Advance temperature at new time level $(n+1)\,\Delta t$.

2. Form the source terms $S_u^{n,n-1}$ and $S_w^{n,n-1}$ that do not incorporate pressure gradients. In order to retain the second order accuracy in time, the body force term in (1-3) is evaluated as $0.5*(\theta^{n+1} + \theta^n)$.

3. Form the source term for the Poisson's equation for pressure by computing $(\partial/\partial x)\, S_u^{n,n-1} + (\partial/\partial z)\, S_w^{n,n-1}$ in the spectral space.

4. Determine a trial pressure distribution $\bar{p}_t$ that satisfies (8-1). In our particular problem $\bar{p}_t$ can be taken as zero on ∂D.

5. Solve the Poisson's equation for pressure.

6. Form the gradients of the pressure field that are added to $S_u^{n,n-1}$ and $S_w^{n,n-1}$.

7. Advance both components of velocity field at time $(n+1)\,\Delta t$ in spectral space.

8. Form the divergence of the velocity field in the spectral space and get its values in physical space at the set of collocation points $\{C_i\}$ on the boundary ∂D that is $\bar{\omega}_t$.

9. Get $\bar{p}_c$ from the inversion of the linear system $Q\bar{p}_c = -\bar{\omega}_t$.

10. Form the true pressure distribution at the boundary $\bar{p}_c + \bar{p}_t$ and repeat steps 5, 6 and 7.

Two points are worth mentioning: first, the overall scheme is clearly formally second-order accurate in time. Second, since the source terms for the two components of velocity are evaluated only once and also because of the great efficiency of the Helmholtz solver, the increase in computing time over a direct algorithm where steps 5, 6 and 7 would be done only once is not prohibitive.

4. Results and Discussion

4.1. *Validation of the Code*

In order to demonstrate the validity of our code and to check its accuracy, we have computed the different solutions of the above described problem for four values of the Rayleigh number $\mathrm{Ra} = 10^3$, 10^4, 10^5 and 10^6. The Prandtl number is set to 0.71. These solutions were the object of a comparison problem proposed in 1979 [11] and on this occasion, De Vahl Davis [4] produced a benchmark solution, one of the most accurate solutions available for this problem. This benchmark solution was obtained after a local Richardson extrapolation was applied to solutions calculated by means of finite-difference techniques of second-order accuracy on meshes of different size. The finest mesh used to compute the solutions for $\mathrm{Ra} = 10^5$ and 10^6 was 81×81 points. We have reported in Table I the characteristic values of the benchmark solution together with two sets of results produced with our code: the first set was computed using 17×17 modes in each direction ($L = M = 16$), whereas the second one corresponds to 33×33 modes ($L = M = 32$). It is worth remarking that up to $\mathrm{Ra} = 10^5$, the 17×17 solutions are in excellent agreement with both the benchmark and the 33×33 solutions which proves that a 17×17 spectral expansion is sufficient for these values of the Rayleigh

581/57/2-5

TABLE I

	Ra											
	10^3	10^4	10^5	10^6	10^3	10^4	10^5	10^6	10^3	10^4	10^5	10^6
$\Psi_{\frac{1}{2}\frac{1}{2}}$	1.174	5.071	9.111	16.32	1.1746	5.074	9.118	16.95	1.1746	5.0736	9.123	16.37
Ψ max	—	—	9.612	16.750	—	—	9.625	17.02	—	—	9.621	16.806
X/Z	—	—	0.285/0.601	0.151/0.547	—	—	0.284/0.602	0.147/0.568	—	—	0.285/0.601	0.151/0.547
U max	3.649	16.178	34.73	64.63	3.6497	16.186	34.85	69.76	3.6494	16.183	34.76	64.81
Z	0.813	0.823	0.855	0.850	0.813	0.823	0.854	0.84	0.813	0.823	0.855	0.850
W max	3.697	19.617	68.59	219.36	3.6978	19.633	68.40	219.76	3.6974	19.629	68.65	220.57
X	0.178	0.119	0.066	0.0379	0.178	0.119	0.066	0.0395	0.178	0.119	0.066	0.0378
Nu $\frac{1}{2}$	1.118	2.243	4.519	8.799	1.1178	2.245	4.532	8.52	1.1178	2.245	4.526	8.814
Nu 0	1.117	2.238	4.509	8.817	1.1178	2.245	4.521	8.97	1.1178	2.245	4.521	8.826
Nu max	1.505	3.528	7.717	18.230	1.506	3.531	7.726	18.15	1.506	3.531	7.720	17.533
Z	0.092	0.143	0.081	0.0417	0.088	0.144	0.083	0.04	0.088	0.144	0.082	0.039
Nu min	0.692	0.586	0.729	0.989	0.691	0.585	0.728	0.88	0.691	0.585	0.728	0.979
Z	1	1	1	1	1	1	1	0.98	1	1	1	1
	Solution after [4]				17×17 modes				33×33 modes			

number. The fact that the solution 17×17 for $\mathrm{Ra} = 10^6$ is more than qualitative is also noteworthy. For the higher values of the Rayleigh number, the solution 33×33 is in very close agreement with the benchmark solution except for the maximum value of the Nusselt number on the hot wall. To close the discussion on this point of disagreement, we have computed the two solutions $\mathrm{Ra} = 10^5$ and 10^6 with a 65×65 modes code. The results are presented in Table II and show that the values obtained with the 33×33 modes code are confirmed to the third decimal place (the largest relative difference is 0.002). All these results confirm (if still needed) the spectacular rate of convergence of expansions in series of Chebyshev polynomials.

A further proof of the convergence of the spectral spatial expansions can be obtained by looking at the distribution of the spectral coefficients of the different variables of a solution. Let us consider, for instance, the steady-state temperature field corresponding to a Rayleigh number of 10^6 obtained with the 33×33 modes code ($L = M = 32$). Let θ_{lm}, $(l, m) \in (0,..., L) \times (0,..., L)$, be the two-dimensional array of spectral coefficients of this temperature field. We show in Fig. 2 the behaviour of $a_k = \sup_{k=l+m}(\log |\theta_{lm}|)$ as a function of k where k belongs to $(0,..., 2L)$. This particular function clearly shows that the solution of Eqs. (1-1)–(1-5) is symmetric with respect to the center of the computational domain. Accordingly the spectral coefficients θ_{lm} should be identically zero for all the couples (l, m) such as $l + m$ is even except for the mean value $l = m = 0$. In Fig. 2 such coefficients are figured with squares. The meaningful coefficients figured with triangles are such

TABLE II

	Ra		
	10^5	10^6	10^7
$\Psi_{\frac{1}{2}\frac{1}{2}}$	9.119	16.39	29.27
Ψ max	9.619	16.811	30.17: 0.086/0.556
$x - z$	0.285/0.601	0.151/0.547	26.63: 0.125/0.875
U max	34.75	64.83	148.8
z	0.855	0.850	0.879
W max	68.64	220.56	699.3
x	0.066	0.0375	0.0213
Nu $\frac{1}{2}$	4.523	8.826	16.51
Nu 0	4.522	8.825	16.52
Nu max	7.720	17.536	39.37
z	0.082	0.039	0.0180
Nu min	0.728	0.979	1.367
z	1	1	1
		65×65 modes	

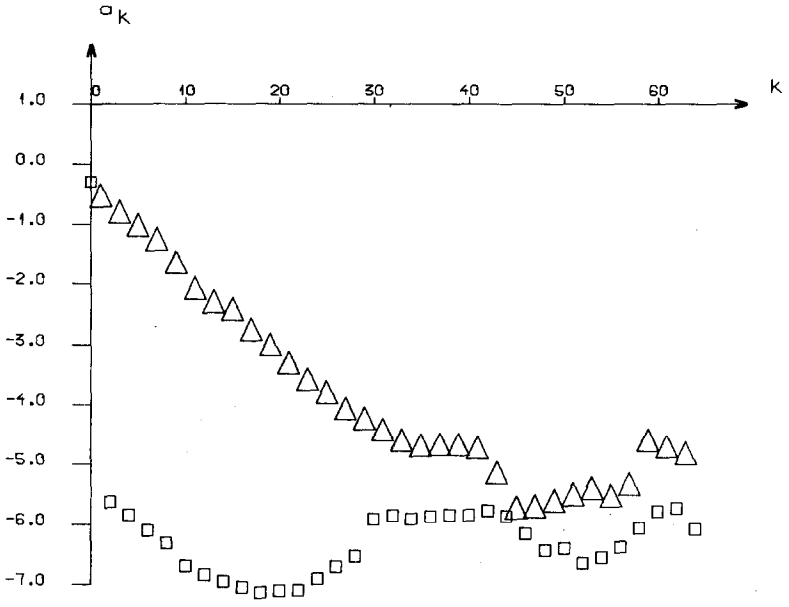

FIG. 2. Behaviour of spectral coefficients of the temperature field for $\mathrm{Ra} = 10^6$.

as $l+m$ is odd, and one sees that a_k decays almost linearly for $0 \leqslant k \leqslant L$, and then remains approximately constant for k larger than L. The 4 to 5 orders in magnitude in the difference between the largest and smallest coefficients is a further confirmation of the convergence of the spectral expansion for this temperature field.

4.2. *Computing Time and Time-Step Limitations*

All the above solutions have been obtained by integrating during a sufficiently long time in order to get the steady-state solutions corresponding to the 4 different Rayleigh numbers. In this respect the work by Patterson and Imberger [12] is of importance since it gives an estimate of the dimensionless integration time t_* needed to reach a steady-state solution (though strictly speaking, their analysis is limited to values of the Prandtl number larger than unity). For the two higher values of the Rayleigh number, the value of t_* is 1/Pr in the dimensionless unit considered and a steady state is achieved after internal gravity waves that are generated in the early stages of the transient period are damped out. This means that, since the time step we can choose is restricted by the stability limit of the Adams–Bashforth scheme, it is quite costly to get the steady-state solutions. To be specific, the four 33×33 solutions in Table I needed 4.5 hours of CPU time on an IBM 370/168. The 33×33 code runs in 2.8 seconds per time step on this machine. The useable time steps were 4×10^{-4} for $\mathrm{Ra} = 10^3$ and 10^4 and 8×10^{-5} for $\mathrm{Ra} = 10^5$ and 10^6. We have checked, by freezing the velocity field and going on with the integration of the temperature field alone, that these limits correspond effectively

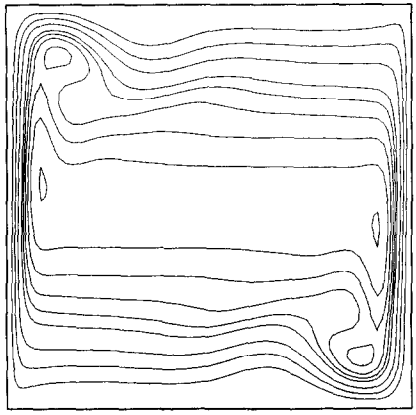

FIG. 3. Streamfunction $Ra = 10^7$. Isovalues are (5, 10, 15, 20, 22, 24, 26, 28, 30).

with the linear stability limits of the *ABCN* time-stepping scheme. The 65×65 modes code runs in 12 sec per time step on the same machine and needs 0.3 sec per time step on the CRAY-1*S*.

4.3. *Solution at* $Ra = 10^7$

In Table II we have also reported the steady-state solution obtained for $Ra = 10^7$. The calculation was started from the solution for $Ra = 10^6$, and it was necessary to choose a time step as small as 7×10^{-6}. This means that it would have been necessary to integrate for on the order of 10^5 time steps to attain the steady-state solution. We could reduce this number appreciably by averaging the velocity and temperature fields over several periods of oscillations of the internal gravity waves, and then reinitializing a computing sequence over which the solution could be con-

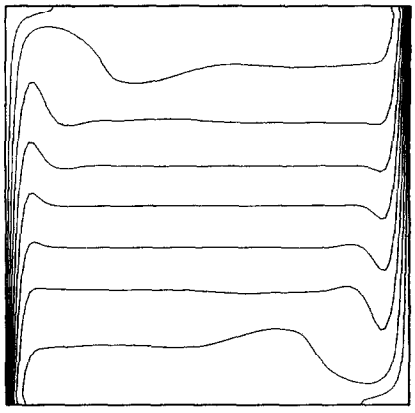

FIG. 4. Isotherms $Ra = 10^7$. Isovalues are 0 (0.1) 1.

sidered as steady. The residual oscillations on the different quantities monitored were less than 10^{-3}. The period of the oscillations in this case is 3.52×10^{-3}. This is exactly the value that was obtained numericaly by Lauriat [13], whereas the theoretical prediction from [12] is 3.33×10^{-3}. We present in Figs. 3 and 4 the steady-state stream function and isothermal fields. Two relative extrema of the stream function can be distinguished, the values of which are reported in Table II. It is interesting to note that expansions in series of Chebyshev polynomials are indeed well suited to resolve the very thin boundary layers adjacent to the vertical boundaries. In this case, when $\mathrm{Ra} = 10^7$ and $L = M = 64$, there are five collocation points between the boundary and the point where the vertical velocity component reaches its maximum value at mid-height of the cavity. This is due to the fact that the mesh spacing is of order $1/L^2$ for the collocation points near to the boundaries of the computational domain.

4.4. *Solution at* $\mathrm{Ra} = 4 \times 10^7$

Since our objective was to reach the domain of time-dependent solutions, we decided, according to the results of Gill and Davey [3], to run a case with a Rayleigh number set to 4×10^7. Starting from the solution for $\mathrm{Ra} = 10^7$, we had to reduce the time-step size in the early stages to 10^{-6}, but after some time of integration its value could be increased to 2×10^{-6}. We show in Fig. 5 the behaviour of the Nusselt numbers at the wall Nu_w and in the center region of the cavity

$$\mathrm{Nu}_c = \int^1 \left(u\theta - \frac{\partial \theta}{\partial x} \right) (x = 0.5, z)\, dz.$$

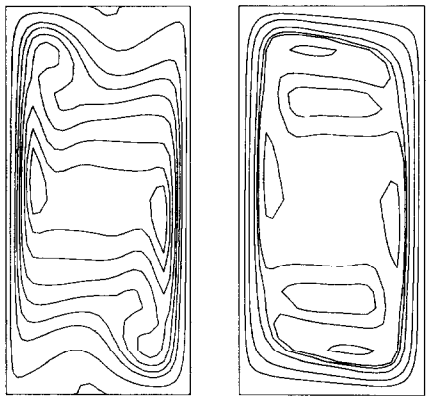

FIG. 8. Streamline patterns ($Ra = 2 \times 10^6$, $A = 2$) with adiabatic (left) and perfectly conducting (right) thermal boundary conditions on the horizontal walls.

case, there are still four collocation points between the boundary and the point where the vertical velocity component reaches its maximum value.

Two important points are worth mentioning:

1. The existence of a counterclockwise motion (the primary circulation is clockwise) which can to some extent be compared to the tertiary motion described by Elder [14].

2. The existence of a detached region along the upper and lower adiabatic walls. These detached regions were already present periodically in the transient solution from $Ra = 10^6$ to 10^7 but did not persist at steady state. The origin of this phenomenon, which lies probably in a complex balance between inertial, buoyant and pressure forces, is still unclear. Suffice to say, the thermal boundary condition on the horizontal walls plays an essential role in its appearance, as can be seen from Fig. 8, which shows the streamline patterns in a cavity with $Ra = 2 \times 10^6$ and $A = 2$ corresponding to two different types of boundary conditions. The left plot which exhibits the detached region corresponds to adiabatic horizontal walls, whereas the right plot corresponds to a cavity for which a linear temperature distribution between the cold and hot walls was assumed. These two solutions were obtained with a 33×33 modes code.

The question of the existence of time-dependent solutions to the two-dimensional problem has also been investigated by Bergholz [15]. The key parameter in his study is the thermal stratification parameter $\tau = (1/4.h.\mathrm{Ra})^{0.25}$, where h is the dimensionless vertical temperature gradient in the center of the cavity. The value of the stratification parameter computed from our solution is about 50. This value is not in the range covered by Bergholz, who stopped his computations at a value of 12 for a Prandtl number of 0.73, and this does not permit any useful comparison.

5. Conclusion

In this paper we have presented a numerical algorithm for the integration of the Navier–Stokes equations of a Boussinesq fluid enclosed in a two-dimensional upright cavity. The algorithm combines spatial spectral expansions in truncated series of Chebyshev polynomials with a second-order time-stepping scheme. However, due to the explicit treatment of the convective terms, the time integration is only conditionally stable. For the computation of natural convection in enclosed cavities, this results in rather long computing times since it is necessary to damp internal gravity waves before achieving a steady state. This clearly shows the interest for improved stability algorithms of the kind suggested by Orszag [16]. We have nonetheless been able to show that the range of steady-state solutions to the problem of natural convection of air enclosed in a square differentially heated cavity extends beyond the critical values obtained from a linear stability analysis of the buoyancy layer.

Appendix

Let $f(x, z)$ be a continuous function defined on $D = [-1, 1] \times [-1, 1]$ and f_{LM} its truncated development on the basis of Chebyshev polynomials

$$f(x, z) \approx f_{LM}(x, z) = \sum_{l=0}^{L} \sum_{m=0}^{L} f_{lm} T_l(x)\, T_m(z).$$

The collocation points related to the use of Chebyshev polynomials are the couples $(x_i, z_j) = (\cos(i\pi/M), \cos(j\pi/M))$, where $(i, j) \in (0,..., L) \times (0,..., L)$. Let $\{C_i\}$ be the set of collocation points that belong to the boundary of D minus the four corners.

The problem that we want to solve is the following: Given the values of f on $\{C_i\}$, how can we determine the values of f at the four corners so that the laplacian of f at these points takes on prescribed values?

Let E, F, G, H be the corners of the computational domain of respective coordinates $(1, 1)$, $(-1, 1)$, $(-1, -1)$, $(1, -1)$ and f_E, f_F, f_G, f_H the values of $f(x, z)$ at each corresponding point.

Let us also introduce the notation:

$$p(x) = f(x, z = 1) \quad \text{and} \quad q(x) = f(x, z = -1)$$
$$r(z) = f(x = 1, z) \quad \text{and} \quad s(z) = f(x = -1, z).$$

The laplacian of f at E then reads

$$\Delta f_E = p''(x)\,|_{x=1} + r''(z)\,|_{z=1}.$$

$p(x)$ (resp. $r(z)$) is known through its values at the collocation points on EF (resp.

EH), that is, $p(x) = (f_E, p(x_1),..., p(x_{L-1}), f_F)$. Since $p''(x)$ in $x = 1$ depends linearly on f_E and f_F, we express

$$p(x) = f_E \cdot (1, 0, 0,..., 0) + f_F \cdot (0, 0,..., 0, 1) + (0, p(x_1),..., p(x_{L-1}), 0)$$

and develop respectively

$$(1, 0,..., 0, 0) = \sum_{n=0}^{L} a_n T_n(x), \tag{A-1}$$

$$(0, 0,..., 0, 1) = \sum_{n=0}^{L} b_n T_n(x), \tag{A-2}$$

$$(0, p(x_1),..., p(x_{L-1}), 0) = \sum_{n=0}^{L} p_n T_n(x). \tag{A-3}$$

If g_n are the Chebyshev spectral coefficients of a function $g(x)$, let $g_n^{(2)}$ be the spectral coefficients of $g''(x)$. We can then form

$$\sum_{n=0}^{L} a_n^{(2)}, \quad \sum_{n=0}^{L} (-1)^n a_n^{(2)}, \quad \sum_{n=0}^{L} b_n^{(2)}, \quad \sum_{n=0}^{L} (-1)^n b_n^{(2)}, \quad \sum_{n=0}^{L} p_n^{(2)}, \quad \sum_{n=0}^{L} (-1)^n p_n^{(2)}$$

that represent the values of the second derivative of the functions defined by (A-1)–(A-3) respectively in 1 and -1.

It is easy to see that $\sum_n a_n^{(2)} = \sum_n (-1)^n b_n^{(2)} = \alpha$ and that $\sum_n (-1)^n a_n^{(2)} = \sum_n b_n^{(2)} = \beta$, where the summation indices n run from 0 to L. We have then

$$p''(x)\,|_{x=1} = \alpha \cdot f_E + \beta \cdot f_F + \sum_n p_n^{(2)}$$

and

$$r''(z)\,|_{z=1} = \alpha \cdot f_E + \beta \cdot f_H + \sum_n r_n^{(2)}$$

thus giving

$$\Delta f_E = 2\alpha \cdot f_E + \beta \cdot f_F + \beta \cdot f_H + \sum_n (p_n^{(2)} + r_n^{(2)}).$$

Repeating the same procedure at each of the corners of D, allows us to built the linear system of equations

$$\begin{bmatrix} 2\alpha & \beta & 0 & \beta \\ \beta & 2\alpha & \beta & 0 \\ 0 & \beta & 2\alpha & \beta \\ \beta & 0 & \beta & 2\alpha \end{bmatrix} \begin{bmatrix} f_E \\ f_F \\ f_G \\ f_H \end{bmatrix} = \begin{bmatrix} L_E - \sum_n (p_n^{(2)} + r_n^{(2)}) \\ L_F - \sum_n ((-1)^n p_n^{(2)} + s_n^{(2)}) \\ L_G - \sum_n ((-1)^n q_n^{(2)} + (-1)^n s_n^{(2)}) \\ L_H - \sum_n (q_n^{(2)} + (-1)^n r_n^{(2)}) \end{bmatrix}$$

where L_E, L_F, L_G, L_H stand for the desired values of the laplacian at each respective corner.

ACKNOWLEDGMENTS

This work was performed under CNRSs ATP Mathématiques appliquées et methodes numériques performantes and ATP CRAY. We would like to thank Dr. Meneguzzi for providing access to the TEMPERTON FFT package.

REFERENCES

1. S. A. ORSZAG, *J. Fluid Mech.* **50** (1971), 689.
2. S. A. ORSZAG. *Stud. Appl. Math.* **50** (1971), 293.
3. A. E. GILL AND A. DAVEY, *J. Fluid Mech.* **35** (1969), 775.
4. G. DE VAHL DAVIS, Report 1981/FMT/University of New South Wales, School of Mech. and Ind. Eng.
5. D. GOTTLIEB AND S. A. ORSZAG, NSF-CBMS Monograph No. 26, Soc. Ind. and Appl. Math., Philadelphia, 1977.
6. P. MOIN AND J. KIM, *J. Comput. Phys.* **35** (1980), 381.
7. S. A. ORSZAG AND L. C. KELLS, *J. Fluid Mech.* **96** (1980), 159.
8. J. B. MCLAUGHLIN AND S. A. ORSZAG, *J. Fluid Mech.* **122** (1982), 123.
9. L. KLEISER AND U. SCHUMANN, "Notes on Numerical Fluid Mechanics" (E. H. Hirschel, Ed.), Vol. 3p. 165, Vieweg, 1980.
10. D. B. HAIDVOGEL AND T. ZANG, *J. Comput. Phys.* **30** (1979), 167.
11. *J. Fluid Mech.* **95** (1979), Part 4 (inside back cover).
12. J. PATTERSON AND J. IMBERGER, *J. Fluid Mech.* **100** (1980), 65.
13. G. LAURIAT, Thèse Doctorat d'Etat, Université Paris 6, Dec. 1981.
14. J. W. ELDER, *J. Fluid Mech.* **23** (1965), 77.
15. R. F. BERGHOLZ, *J. Fluid Mech.* **84** (1978), 743.
16. S. A. ORSZAG, *J. Comput. Phys.* **37** (1980), 70.